
Towards Generalizable Reinforcement Learning via Causality-Guided Self-Adaptive Representations

Yupei Yang¹, Biwei Huang^{2*}, Fan Feng³, Xinyue Wang², Shikui Tu^{1*}, Lei Xu^{1,4}

¹Shanghai Jiao Tong University, ²University of California San Diego,

³City University of Hong Kong, ⁴Guangdong Institute of Intelligence Science and Technology

{yupei_yang, tushikui, leixu}@sjtu.edu.cn,
{bih007, xiw159}@ucsd.edu, ffeng1017@gmail.com

Abstract

General intelligence requires quick adaption across tasks. While existing reinforcement learning (RL) methods have made progress in generalization, they typically assume only distribution changes between source and target domains. In this paper, we explore a wider range of scenarios where both the distribution and environment spaces may change. For example, in Atari games, we train agents to generalize to tasks with different levels of mode and difficulty, where there could be new state or action variables that never occurred in previous environments. To address this challenging setting, we introduce a *causality-guided self-adaptive representation*-based approach, called CSR, that equips the agent to generalize effectively and efficiently across a sequence of tasks with evolving dynamics. Specifically, we employ causal representation learning to characterize the latent causal variables and world models within the RL system. Such compact causal representations uncover the structural relationships among variables, enabling the agent to autonomously determine whether changes in the environment stem from distribution shifts or variations in space, and to precisely locate these changes. We then devise a three-step strategy to fine-tune the model under different scenarios accordingly. Empirical experiments show that CSR efficiently adapts to the target domains with only a few samples and outperforms state-of-the-art baselines on a wide range of scenarios, including our simulated environments, Cartpole, and Atari games.

1 Introduction

In recent years, deep reinforcement learning (DRL) [1] has made incredible progress in various domains [2, 3]. Most of these works involve learning policies separately for fixed tasks. However, many practical scenarios often have a sequence of tasks with evolving dynamics. Instead of learning each task from scratch, humans possess the ability to discover the similarity between tasks and quickly generalize learned skills to new environments [4, 5]. Therefore, it is essential to build a system where agents can also perform reliable and interpretable generalizations to advance towards general artificial intelligence [6].

A straightforward solution is policy adaptation, i.e., leveraging the strategies developed in source tasks and adapting them to the target task as effective as possible [7]. Approaches along this line include but are not limited to finetuning [8], reward shaping [9], importance reweighting [10], learning robust policies [11, 12], sim2real [13], adaptive RL [14], and subspace building [15]. However, these algorithms often rely on an assumption that all the source and target domains have the same state and action space while ignoring the out-of-distribution scenarios which are more common in practice [16, 17].

*corresponding author

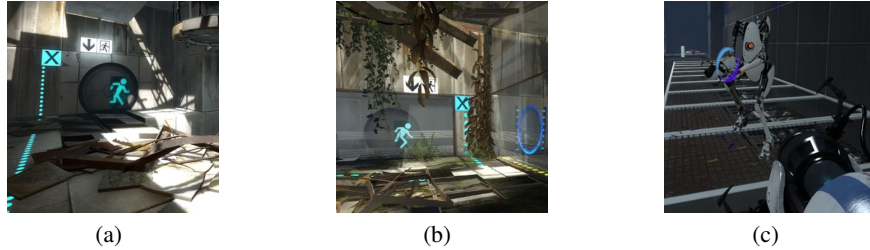


Figure 1: Different game levels in "Portal 2": (a) Level 1: Escape in a room with simple layouts; (b) Escape in a room with complex layouts; (c) Level 3: A robot stops you from escaping.

In this paper, we expand the application of RL beyond its traditional confines by exploring its adaptability in broader contexts. Specifically, our investigation focuses on policy adaptation in two distinct scenarios:

1. *Distribution shifts*: the source and target data originate from the same environment space but exhibit differences in their distributions, e.g. changes in transition, observation or reward functions;
2. *State/Action space expansions*: the source and target data are collected from different environment spaces, e.g. they differ in the latent state or action spaces.

These scenarios frequently occur in practical settings. To illustrate, we reference the popular video game "Portal 2". As shown in Fig. 1, players must use a portal gun to create interconnected gateways, aiding their advancement to new areas and solving various mechanisms and puzzles. Initially, the game environments are relatively straightforward (see Fig. 1(a)). As players progress through levels, the environments become more complex (see Fig. 1(b)), requiring players to continually adapt their strategies to the changing room settings — this exemplifies distribution shifts. Eventually, a variety of robots appear, obstructing and attacking the player, and the system introduces new tools (see Fig. 1(c)). To prevail, players must master these new tools to navigate past the robots' disruptions — this scenario belongs to state/action space expansions.

We propose a **Causality-guided Self-adaptive Representation-based** approach, termed CSR, to address this problem for partially observable Markov decision processes (POMDPs). Considering that the raw observations are often reflections of the underlying state variables, we employ causal representation learning [18–23] to identify the latent causal variables in the RL system, as well as the structural relationships among them. By leveraging such representations, we can automatically determine what and where the changes are. To be specific, we first augment the world models [24, 25] by including a task-specific change factor θ to capture distribution shifts, e.g., θ can characterize the changes in transition dynamics due to varying room layouts in "Portal 2". If the introduction of θ can well explain the current observation, it is enough to keep previously learned causal variables and merely update a few parameters in the causal model. Otherwise, it implies that the current task differs from previously seen ones in the environment spaces, we then expand the causal graph by adding new causal variables and re-estimate the causal model. Finally, we remove some irrelevant causal variables that are redundant for policy learning (i.e., no direct edges to rewards) according to the identified causal structures. This three-step strategy enables us to capture the changes in the environments for both scenarios in a self-adaptive manner and make the most of learned causal knowledge for low-cost policy transfer. Our key contributions are summarized below:

- We investigate a broader scenario towards generalizable reinforcement learning, where changes occur not only in the distributions but also in the environment spaces of latent variables, and propose a causality-guided self-adaptive representation-based approach to tackle this challenge.
- To characterize both the causal representations and environmental changes, we construct a world model that explicitly uncovers the structural relationships among latent variables in the RL system.
- By leveraging the compact causal representations, we devise a three-step strategy that can identify where the changes of the environment take place and add new causal variables autonomously if necessary. With this self-adaptive strategy, we achieve low-cost policy transfer by updating only a few parameters in the causal model.

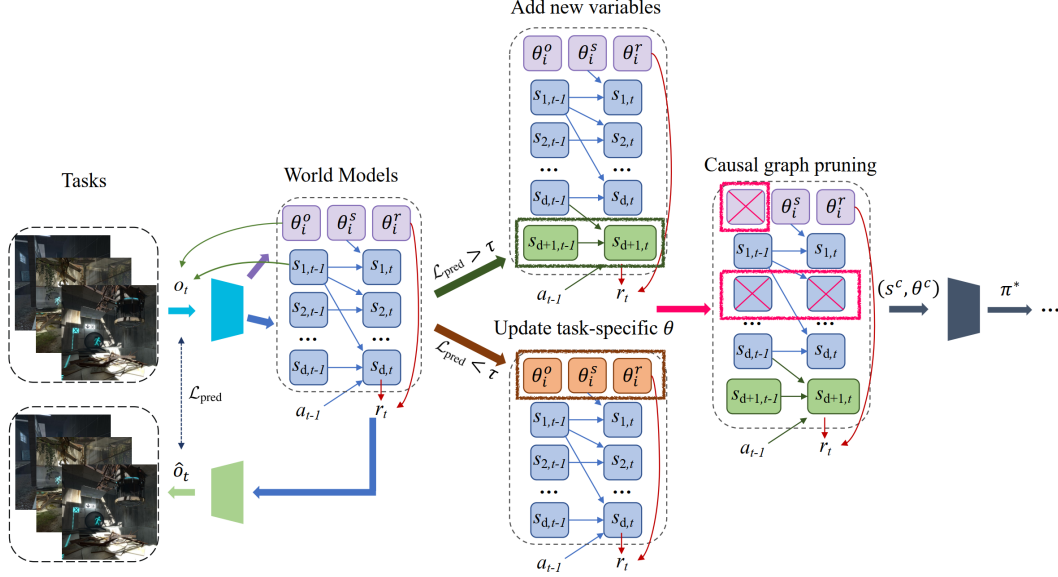


Figure 2: The overall CSR framework. For each target task, we first use the prediction error, $\mathcal{L}_{\text{pred}}$, to determine whether it involves distribution shifts or space shifts. We then adjust the model accordingly by updating the task-specific change factor θ_i , or by adding new variables. Finally, we conduct causal graph pruning that removes variables unnecessary for the current task. Based on such compact causal representations, we can efficiently implement policy adaptation in a self-adaptive manner.

2 World Model with Causality-Guided Self-adaptive Representations

We consider generalizable RL that aims to effectively transfer knowledge across tasks, allowing the model to leverage patterns learned from a set of source tasks while adapting to the dynamics of a target task. Each task \mathcal{M}_i is characterized by $\langle \mathcal{S}_i, \mathcal{A}_i, \mathcal{O}_i, R_i, T_i, \phi_i, \gamma_i \rangle$, where \mathcal{S}_i represents the latent state space, \mathcal{A}_i is the action space, \mathcal{O}_i is the observation space, $R_i: \mathcal{S}_i \times \mathcal{A}_i \rightarrow \mathbb{R}$ is the reward function, $T_i: \mathcal{S}_i \times \mathcal{A}_i \rightarrow P(\mathcal{S}_i)$ is the transition function, $\phi_i: \mathcal{S}_i \times \mathcal{A}_i \rightarrow P(\mathcal{O}_i)$ is the observation function, and γ_i is the discount factor. By leveraging experiences from previously encountered tasks $\{\mathcal{M}_j\}_{j=1}^{i-1}$, the objective is to adapt the optimal policy π^* that maximizes cumulative rewards to the target task \mathcal{M}_i . Here, we consider tasks arriving incrementally in the sequence $\langle \mathcal{M}_1, \dots, \mathcal{M}_N \rangle$ over time periods $\langle \mathcal{T}_1, \dots, \mathcal{T}_N \rangle$. In each period \mathcal{T}_i , only a replay buffer containing sequences $\{\langle o_t, a_t, r_t \rangle\}_{t=1}^{\mathcal{T}_i}$ from the current task \mathcal{M}_i is available, representing an online setting. While tasks can also be presented offline with predefined source and target tasks, the online framework more closely mirrors human learning, making it a crucial step towards general intelligence.

In this section, we first construct a world model that explicitly embeds the structural relationships among variables in the RL system, and then we show how to encode the changes in the environment by introducing a domain-specific embedding into the model and leveraging it for policy adaptation.

2.1 Augmenting World Models with Structural Relationships

In POMDPs, extracting latent state representations from high-dimensional observations is crucial for enhancing the efficiency of the decision-making process. World models address this challenge by learning a generative model, which enables agents to predict future states through imagination. These methods typically consider all extracted representations of state variables equally important for policy learning, thereby utilizing all available information regardless of its relevance to the current task. However, real-world tasks often require a focus on specific information. Still consider the game "Portal 2", where players use "Propulsion Gel" to accelerate movement and "Repulsion Gel" for high jumps. In tasks that require rapid movement through different rooms, "Propulsion Gel" is more appropriate. Conversely, when the objective is to reach higher elevations, "Repulsion Gel" becomes

essential. Hence, it is essential for agents to understand and focus on task-specific aspects to facilitate effective knowledge transfer by selectively using minimal sufficient information.

To this end, we adopt a causal state representation learning approach that not only enables us to extract state representations, but also to discover structural relationships over the variables. Suppose we observe sequences $\{\langle o_t, a_t, r_t \rangle\}_{t \in \mathcal{T}_i}$ for task \mathcal{M}_i , and denote the underlying causal latent states by $s_t \in \mathcal{S}_i$, we formulate the world model into:

$$\begin{cases} \text{observation model:} & p_\phi(o_t | D^{s \rightarrow o} \odot s_t) \\ \text{reward model:} & p_\phi(r_t | D^{s \rightarrow r} \odot s_t) \\ \text{transition model:} & p_\beta(s_{k,t} | D_k^{s \rightarrow s} \odot s_{t-1}, D_k^{a \rightarrow s} \odot a_{t-1}), \text{ for } k = 1, \dots, d \\ \text{representation model:} & q_\alpha(s_t | s_{t-1}, a_{t-1}, o_t), \end{cases} \quad (1)$$

where $s_t = (s_{1,t}, \dots, s_{d,t})$, \odot is the element-wise product, and $D^{\cdot \rightarrow \cdot}$ denote binary masks indicating structural relationships over variables. For instance, if the j -th element of $D^{s \rightarrow o} \in \{0, 1\}^{d \times 1}$ in Eq. (1) is 1, it indicates a causal edge from the state variable $s_{j,t}$ to the current observation signal o_t , i.e., $s_{j,t}$ is one of the parents of o_t . Consequently, we are supposed to retain $s_{j,t}$ for the observation model. Otherwise, if $D_j^{s \rightarrow o} = 0$, then $s_{j,t}$ should be removed from the causal model. Section 3.3 further discusses the estimation procedures for the structural matrices D , as well as the corresponding pruning process of the causal model. By learning such causal representations, we can explicitly characterize the decisive factors within each task. However, given that the underlying dynamics often vary across tasks, merely identifying which variables are useful is insufficient. We must also determine how these variables change with the environment for better generalization.

2.2 Characterization of Environmental Changes in a Compact Way

To address the above need, we now shift our focus to demonstrating how the world model can be modified to ensure robust generalization across the two challenging scenarios, respectively.

Characterization of Distribution Shifts. To explain the impact of distribution shifts, it is widely recognized that changes in the environmental distribution are often caused by modifications in a few specific factors within the data generation process [26, 19]. For example, in "Portal 2", shifts in the environment might only result from changes in the room layouts (L_r), with all other settings remaining the same. Therefore, To better characterize these shifts, following Huang et al. [14], we introduce a domain-specific change factor, θ , that captures the variations across different domains. Concurrently, we leverage s_t to identify the domain-shared latent variables of the environments. This leads us to reformulate Eq. (1) as follows:

$$\begin{cases} \text{observation model:} & p_\phi(o_t | D^{s \rightarrow o} \odot s_t, D^{\theta_i \rightarrow o} \odot \theta_i^o) \\ \text{reward model:} & p_\phi(r_t | D^{s \rightarrow r} \odot s_t, D^{\theta_i \rightarrow r} \odot \theta_i^r) \\ \text{transition model:} & p_\beta(s_{k,t} | D_k^{s \rightarrow s} \odot s_{t-1}, D_k^{\theta_i \rightarrow s} \odot \theta_i^s, D_k^{a \rightarrow s} \odot a_{t-1}), \text{ for } k = 1, \dots, d \\ \text{representation model:} & q_\alpha(s_t | s_{t-1}, \theta_i, a_{t-1}, o_t). \end{cases} \quad (2)$$

Here, $\theta_i = \{\theta_i^o, \theta_i^r, \theta_i^s\}$ represents the low-dimensional latent variables that capture changes in the observation model, reward model, and transition model, respectively. In the "Portal 2" example, this allows us to make quick adaptations by re-estimating $\theta_i = L_r$ in the target domain.

Characterization of State/Action Space Expansion. For the space expansion scenario, instead of modifying the model's formulation, we are supposed to add new variables to the current causal model. The key challenge here is to determine whether environmental changes observed in the new collection period \mathcal{T}_i are due to distribution shifts or space variations. We can also tackle this problem using θ : If the introduction of θ can well capture the changes in the current observations, then previous tasks $\{\mathcal{M}_j\}_{j=1}^{i-1}$ and \mathcal{M}_i share the same causal variables but exhibit sparse changes in causal parameters (i.e., distribution shifts). In this case, we only need to store the specific part θ of the causal model for \mathcal{M}_i . However, if the learned representations do not capture the current task effectively, the causal graph must be expanded by adding new causal variables to explain the features unique to \mathcal{M}_i .

Benefits of Explicit Causal Structure. In addition, as described in Section 2.1, upon detecting changes in the environment, we can further leverage structural constraints to prune the causal graph. Essentially, we temporarily disregard variables that are irrelevant to the current task. However, for subsequent tasks, we reassess the structural relationships among the variables, enabling potential reuse. This approach allows us to not only preserve previously acquired information but also maintain

the flexibility needed to customize the minimal sufficient state variables for each task. Details of this strategy are given in Section 3.

2.3 Identifiability of Underlying World Models

Below we provide the identifiability theory under different scenarios in this paper: (1) For source task \mathcal{M}_1 , Theorem 1 establishes the conditions under which the latent variable \mathbf{s}_t and the structural matrices D^\cdot can be identified; (2) For the target task with distribution shifts, Theorem 2 outlines the identifiability of the domain-specific factor θ_i ; (3) For the target task with state space shifts, Theorem 3 specifies the identifiability of the newly added state variables $\mathbf{s}_t^{\text{add}}$; (4) For the target task that includes both distribution shifts and state space shifts, Corollary 1 demonstrates the identifiability of both θ_i and $\mathbf{s}_t^{\text{add}}$. The proofs for Theorem 1 has been given in existing work; we present the proofs for Theorem 2 and Theorem 3, as well as Corollary 1, in Appendix A.

Theorem 1. (*Identifiability of world model in Eq. (1)*). *Suppose there exist mappings g^o and h such that $o_t = g^o(\mathbf{s}_t)$ and $\mathbf{s}_t = h(\hat{\mathbf{s}}_t)$. If the following conditions are satisfied, then \mathbf{s}_t is identifiable up to nonlinear invertible component-wise transformations: (1) g^o is invertible; (2) for any $k_1, k_2 \in \{1, \dots, d\}$ and $k_1 \neq k_2$, $\hat{\mathbf{s}}_{k_1,t}$ and $\hat{\mathbf{s}}_{k_2,t}$ are conditionally independent given $\hat{\mathbf{s}}_{t-1}$; (3) for every possible value of \mathbf{s}_t , the vector functions defined in Eq. (A.1) are linearly independent (see Yao et al. [27], Liu et al. [23]). Furthermore, if the Markov condition and faithfulness assumption hold, then the structural matrices D^\cdot are also identifiable (see Huang et al. [14]).*

Theorem 2. (*Identifiability of θ_i in Eq. (2)*). *Suppose the data generation process encounters distribution shifts as described in Eq. (2). If \mathbf{s}_t and the generative functions g^o, g^r, g^s , defined in Eq. (A.2), are identified, then θ_i and the corresponding structural matrices $D^{\theta_i \rightarrow \cdot}$ are identifiable.*

Theorem 3. (*Identifiability of Expanded State Space*). *Consider the expansion of the state space S by incorporating additional dimensions. Suppose \mathbf{s}_t has already been identified according to Theorem 1, the identifiability of the newly added variables $\mathbf{s}_t^{\text{add}}$ and the additional structural matrices, i.e., $D^{\mathbf{s}^{\text{add}} \rightarrow \cdot}$ and $D^{\cdot \rightarrow \mathbf{s}^{\text{add}}}$, can be established if $\mathbf{s}_t^{\text{add}}$ (1) represents a differentiable function of the observations o_t , i.e., $\mathbf{s}_t^{\text{add}} = f(o_t)$, and (2) fulfills conditions (2) and (3) specified in Theorem 1.*

Corollary 1. (*Identifiability under Multiple Shifts*). *Assume the data generation process involves both distribution shifts and state space shifts that comply with Theorem 2 and Theorem 3, respectively. In this case, both the domain-specific factor θ_i and the newly added state variable $\mathbf{s}_t^{\text{add}}$ are identifiable, up to permutation and nonlinear invertible, component-wise transformations.*

3 A Three-Step Self-Adaptive Strategy for Model Adaptation

In this section, we provide a detailed description of a causality-guided self-adaptive strategy aimed at addressing the environmental changes between source and target tasks, ensuring that models can effectively respond to evolving dynamics. Specifically, we proceed with a three-step strategy: (1) Distribution Shifts Detection, (2) State Space Expansion, and (3) Causal Graph Pruning. Algorithm 1 describes the overall process of our three-step causality-guided self-adaptive representation learning.

Before this, we first give the estimation procedures for the source world models defined in Eq. (2), which follows the state-of-the-art work Dreamer [25, 28]. Given the observations in period \mathcal{T}_i , we maximize the object function \mathcal{J} , defined as $\mathcal{J} = \mathcal{J}_{\text{rec}} - \mathcal{J}_{\text{KL}} + \mathcal{J}_{\text{reg}}$, for model optimization. The reconstruction part \mathcal{J}_{rec} is commonly used to minimize the reconstruction error for the perceived image o_t and the reward r_t , which is defined as

$$\mathcal{J}_{\text{rec}} = \mathbb{E}_{q_\alpha} \left(\sum_{t \in \mathcal{T}_i} \{ \log p_\phi(o_t | D^{\mathbf{s} \rightarrow o} \odot \mathbf{s}_t, D^{\theta_i \rightarrow o} \odot \theta_i^o) + p_\phi(r_t | D^{\mathbf{s} \rightarrow r} \odot \mathbf{s}_t, D^{\theta_i \rightarrow r} \odot \theta_i^r) \} \right).$$

We also consider the KL-divergence constraints \mathcal{J}_{KL} that helps to ensure that the latent representations attain optimal compression of the high-dimensional observations, which is formulated as:

$$\mathcal{J}_{\text{KL}} = \mathbb{E}_{q_\alpha} \left(\sum_{t \in \mathcal{T}_i} \{ \lambda_{\text{KL}} \cdot \text{KL}(q_\alpha(\mathbf{s}_t | \mathbf{s}_{t-1}, \theta_i, a_{t-1}, o_t) \| p_\beta(s_{k,t} | D_k^{\mathbf{s} \rightarrow \mathbf{s}} \odot \mathbf{s}_{t-1}, D_k^{\theta_i \rightarrow \mathbf{s}} \odot \theta_i^s, D_k^{a \rightarrow \mathbf{s}} \odot a_{t-1})) \} \right),$$

where λ_{KL} is the regularization term. Moreover, as explained below in the Section 3.3, we further use \mathcal{J}_{reg} as sparsity constraints that help to identify the binary masks better. Upon implementation, these

Algorithm 1 Towards Generalizable RL through Causality-Guided Self-Adaptive Representations

- 1: **Input:** Task \mathcal{M}_i in period \mathcal{T}_i , World Model W under task \mathcal{M}_{i-1} , Threshold τ^* .
 - 2: Collect multiple rollouts \mathcal{B} from \mathcal{M}_i .
 - 3: **while** generalization **do**
 - 4: *Distribution Shifts Detection:* Fine-tune W with task-specific change factor θ_i and obtain prediction error $\mathcal{L}_{\text{pred}}$ on \mathcal{B} .
 - 5: **if** $\mathcal{L}_{\text{pred}} > \tau^*$ **then**
 - 6: *State Space Expansion:* Introduce new state variables into the graph and update W on \mathcal{B} .
 - 7: **end if**
 - 8: *Causal Graph Pruning:* Remove irrelevant causal variables for \mathcal{M}_i .
 - 9: **end while**
 - 10: **return** Latest model W for task \mathcal{M}_i .
-

three components are jointly optimized for model estimation. During the first task \mathcal{M}_1 , we focus on developing the world models from scratch to capture the compact causal representations effectively. Then, for any subsequent target task \mathcal{M}_i (where $i \geq 2$), our objective shifts to continuously refining the world model to accommodate new tasks according to the following steps.

3.1 Distribution Shifts Detection and Characterization

For each task \mathcal{M}_i , our first goal is to determine if it exhibits any distribution shifts. Therefore, in this step, we exclusively updates the domain-specific part θ_i , while keeping all other parameters unchanged from the previous task \mathcal{M}_{i-1} , to detect whether the distributions have changed. Specifically, we split the change factor, θ_i , into three components: θ_i^o , θ_i^s , and θ_i^r . These components respectively correspond to the domain-specific information of the observation model, transition dynamics, and reward function. Similar to Eq. (1), we also employ the structural matrices, $D^{\theta_i \rightarrow \cdot}$, to capture the causal relationships between θ_i and other variables. For instance, if $D_1^{\theta_i \rightarrow r} = 0$, it indicates that the first component of θ_i does not affect the reward r_t in the current task. We assume that these structural matrices are consistent across all tasks. However, the effect of each connection can differ from one task to another. By adjusting the values of θ_i , we modulate the influence of these connections. Particularly, when θ_i is set to zero, we temporarily switch the related edges off in task \mathcal{M}_i . Drawing from Zhang et al. [29] and Huang et al. [14], we further hypothesize that the value of θ_i remains constant for each task.

If the re-estimated model in this step can well explain the observations in current task, it means that the environment only encounter distribution shifts. Following the recommendations from Khetarpal et al. [30], we adopt forward prediction error [31] as the criteria, defined as

$$\mathcal{L}_{\text{pred}} = \mathbb{E}_{\hat{o}_{t+1} \sim p_\phi} \|\hat{o}_{t+1} - o_{t+1}\|_2^2. \quad (3)$$

A corresponding threshold, τ^* , is established, and if the model’s performance τ is below this expected threshold, it suggests that the causal variables for the current task \mathcal{M}_i were indeed previously encountered in the source tasks, requiring only minor adjustments in some parameters. Thus, incorporating θ_i effectively manages these distribution changes. Conversely, if this is not the case, it suggests that the environmental changes for task \mathcal{M}_i extend beyond mere distribution shifts, prompting us to proceed to the next step.

3.2 State Space Expansion

When the involved domain-specific features θ_i fail to accurately represent the target task \mathcal{M}_i , it becomes essential to incorporate additional causal variables into the existing causal graph to account for the features encountered in the new task. Thus, in this step, we focus on developing strategies to expand the latent state space. Let d' denote the number of causal variables to be added, we first determine the value of d' and introduce new causal features. Following this decision stage, we extend the causal representations from s_t to $s'_t = (s_t, s_t^{\text{add}})$, where $s_t^{\text{add}} = (s_{d+1,t}, \dots, s_{d+d',t})$, by incorporating the additional d' causal variables. Accordingly, only the newly incorporated components are trained from scratch, while the existing parts of the model are fine-tuned. This approach allows us to leverage prior knowledge effectively and achieve low-cost knowledge transfer. Specifically, we propose the following three implementations for state space expansion:

1. *Random (Rnd)*: d' is randomly sampled from a uniform distribution.
2. *Deterministic (Det)*: It sets a constant value for d' . However, this approach may overlook task-specific differences, potentially leading to either insufficient or redundant expansions. To address this, we employ group sparsity regularization on the added parameters after deterministic expansion. This allows for expansion while retaining the capability of shrinking, as demonstrated in Yoon et al. [32] and Li et al. [33].
3. *Self-Adaptive (SA)*: It searches for the value of d' that best fits the current task. To achieve this, we transform expansion into a decision-making process by considering the number of causal variables added to the graph as actions. Inspired by Xu and Zhu [34], we define the state variable to reflect the current causal graph and derive the reward based on changes in predictive accuracy, which is calculated as the differences of the model’s prediction errors, defined in Eq. (3), before and after expansion. Details are given in Appendix B.

It is noteworthy that our method allows for flexibility in the choice of expansion strategies. Intuitively, in our case, the Self-Adaptive approach is most likely to outperform others, and the experimental results in Section 4 further verify this point.

3.3 Causal Graph Pruning

As discussed in Section 2.1, not all variables contribute significantly to policy learning, and the necessary subset also differs between tasks. Therefore, during the generalization process, it is essential to identify the minimal sufficient state variables for each task. Fortunately, with the estimated causal model that explicitly encodes the structural relationships between variables, we can categorize these state variables s_t into the following two classes:

1. *Compact state representation $s_{k,t}^c$* : A variable that either affects the observation o_t , or the reward r_{t+1} , or influences other state variables $s_{j,t+1}$ at the next time step (i.e., $D^{s \rightarrow o} = 1$, $D^{s \rightarrow r} = 1$, or $D_{j,k}^{s \rightarrow s} = 1$).
2. *Non-compact state representation $s_{k,t}^{\bar{c}}$* : A variable that does not meet the criteria for a compact state representation.

Similarly, the change factors θ_i can be classified in the same manner. These definitions help us easily identify compact variables that are useful for policy learning, as they influence observations, rewards, or state transitions. Also, we can selectively remove non-compact ones, thereby pruning the causal graph. In other words, a variable is retained if its corresponding structural constraints D are set to 1. To better characterize the binary masks D and the sparsity of θ_i , we define a regularization term \mathcal{J}_{reg} by leveraging the edge-minimality property [35], formulated as

$$\mathcal{J}_{\text{reg}} = - [\lambda_0 \|D^{s \rightarrow o}\|_1 + \lambda_1 \|D^{s \rightarrow r}\|_1 + \lambda_2 \|D^{s \rightarrow s}\|_1 + \lambda_3 \|D^{a \rightarrow s}\|_1 + \lambda_4 \|D^{\theta_i \rightarrow s}\|_1 + \lambda_5 \|\theta_i\|_1],$$

where λ 's represent the regularization terms. A key advantage is that the regularization term \mathcal{J}_{reg} is integrated into the objective function \mathcal{J} , and thus is optimized concurrently during model training. Therefore, in this step, we only need to perform pruning based on the estimated structural constraints D , eliminating the necessity for additional training.

3.4 Low-Cost Policy Generalization under Different Scenarios

After identifying what and where the changes occur, we are now prepared to perform policy generalization to the target task \mathcal{M}_i . Given that the number of state variables varies between the distribution shifts and state space expansion scenarios, the strategy for policy transfer also differs accordingly.

Inspired by Huang et al. [14], in all these tasks, we incorporate both the domain-shared state representation s_t^c and the domain-specific change factor θ_i^c as inputs to the policy π^* , represented as: $a_t = \pi^*(s_t^c, \theta_i^c)$. This approach enables the agent to accommodate potentially variable aspects of the environment during policy learning. Consequently, given the estimated value of the compact state representation s_t^c and the compact change factor θ_i^c for task \mathcal{M}_i , if the introduction of θ_i^c well represents the target task (i.e., the model’s performance in the Distribution Shifts Detection step meets expectations), we can directly transfer the learned policy \mathcal{M}_i by applying

$$a_t = \pi^*(s_t^c, \theta_i^c).$$

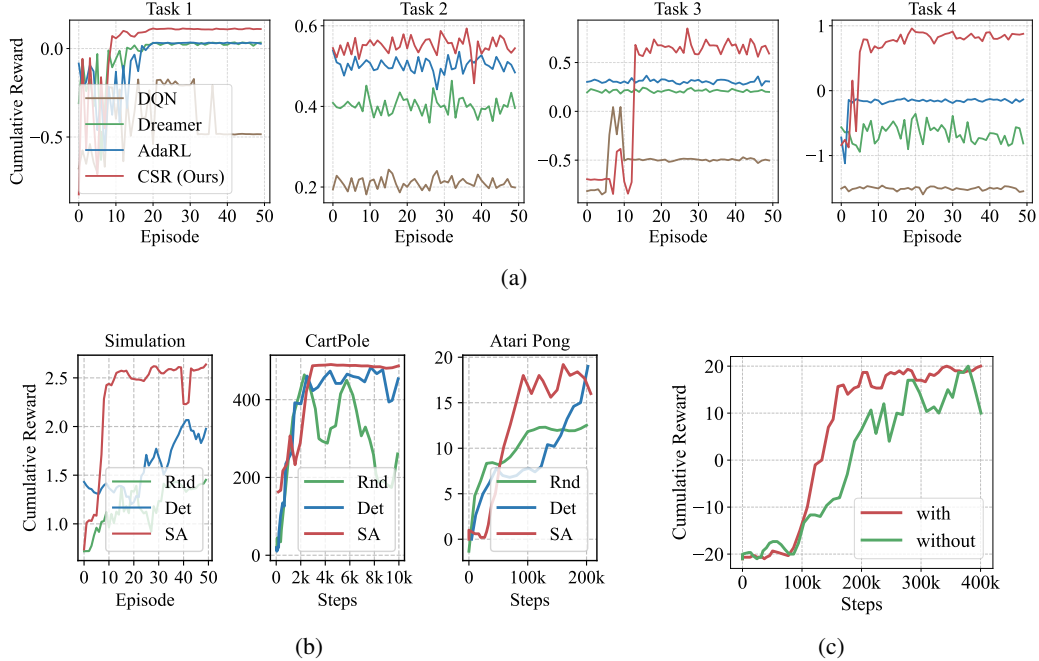


Figure 3: (a) Simulation results; (b) Average training episodic return of CSR with different expansion strategies; (c) Training curves of CSR with/without structural embeddings in the Pong game.

Otherwise, if the causal state representation expands from s_t^c to $s_t^{c'}$, along with the updated change factor $\theta_i^{c'}$, we then relearn the policy $\pi^{*'}$ basing on π^* . Similarly, we train the newly added structures in the policy network while finetuning the original parameters, thereby updating the policy to

$$a_t = \pi^{*'}(s_t^{c'}, \theta_i^{c'}).$$

4 Experiments

We evaluate the generalization capability of CSR on a number of simulated and well-established datasets, including the CartPole and Atari environments in OpenAi Gym [36]. For simulated experiments, we generate synthetic datasets that satisfy the two scenarios with different types of environmental changes. For CartPole, we consider distribution shifts in the task domains with different gravity or cart mass, and space variations by adding cart friction that changes across times. For Atari games, we design the experiments by generating tasks with different game mode and difficulty levels. Such mode and difficulty switches lead to different consequences that changes the game dynamics or introduces new actions into the environment [37]. For all these benchmarks, we evaluate the POMDP case, where the inputs are high-dimensional observations. The baselines used for comparison include model-free DQN [38], SPR [39], model-based Dreamer [28], AdaRL [14], and EfficientZero [40]. All results are averaged over 5 runs, more implementation details can be found in Appendix C.

Simulated Experiments. In our simulated experiments, we conducted a sequence of four tasks (Task 1 to Task 4) following the procedures outlined in Appendix C.1. To evaluate the performance of different methods across varying scenarios, Task 2 focuses exclusively on distribution shifts, Task 3 addresses changes solely within the environment space, and Task 4 combines both distribution and space changes. As shown in Fig. 3(a), CSR consistently outperforms the baselines in adapting to new tasks, particularly excelling in scenarios with space variations. This demonstrates CSR’s ability to accurately detect and adjust to the changes in the environment. Moreover, CSR tends to converge faster toward higher rewards, underscoring its efficiency in data utilization during generalization.

Model	Scores			Minimum Adaptation Steps		
	Task 1	Task 2	Task 3	Task 1	Task 2	Task 3
DQN	44.2 (± 3.1)	61.8 (± 1.7)	39.8 (± 0.5)	50k+	50k+	50k+
Dreamer	500.0 (± 0.0)	397.6 (± 7.2)	311.6 (± 23.3)	50k	4k+	10k+
AdaRL	500.0 (± 0.0)	468.0 (± 2.3)	410.0 (± 3.4)	50k	4k	4k+
CSR (ours)	500.0 (± 0.0)	500.0 (± 0.0)	500.0 (± 0.0)	50k	2k	4k

Table 1: Evaluation results of different approaches in CartPole, with a maximum episode length of 500. "Minimum Adaptation Steps" here reflects the minimal amount of data samples required for the models to generalize to new tasks, as illustrated in Fig. A.3. "+" denotes that the actual adaptation steps required may exceed the listed values due to non-convergence or suboptimal performance of the models.

Task	Random	SPR	Dreamer	AdaRL	EfficientZero	CSR (ours)
Alien	291.9 (± 83.5)	970.3 (± 311.1)	1010.1 (± 339.0)	1147.5 (± 125.7)	557.4 (± 185.9)	1586.9 (± 127.0)
Bank Heist	18.4 (± 2.5)	110.1 (± 128.2)	1313.7 (± 341.5)	1285.4 (± 131.8)	181.0 (± 90.6)	1454.1 (± 178.8)
Crazy Climber	9668.0 (± 2286.0)	32723.5 (± 12125.2)	68026.5 (± 15628.6)	62565.3 (± 15162.2)	56408.3 (± 13388.0)	88306.5 (± 18029.6)
Gopher	235.6 (± 42.5)	294.0 (± 312.1)	5607.3 (± 1982.9)	5359.6 (± 1736.2)	1083.2 (± 784.8)	6718.6 (± 1703.1)
Pong	-20.2 (± 0.1)	-6.8 (± 14.3)	18.0 (± 3.1)	17.6 (± 2.7)	6.8 (± 7.3)	19.6 (± 1.1)

Table 2: Average final scores on the listed Atari 100K games with 5 evaluation seeds.

Cartpole Experiments. CartPole is a classic control task where players move a cart left or right to balance a pendulum attached on it. In our experiments, we consider three consecutive tasks. Task 2 focuses exclusively on distribution shifts by randomly selecting the cart mass and the gravity from $\{0.5, 1, 2.5, 3.5, 4.5\}$ and $\{5, 9.8, 20, 30, 40\}$, respectively. In Tasks 1 and 2, we disregard the influence of the friction force between the cart and the track. In Task 3, however, we introduce this friction into the environment, and vary it over time, which simulates a game scenario where the cart moves on different surfaces, such as ice or grass (see Fig. A.1). We reflect these changes in the image observation by visualizing the track with different colored segments. The evaluation outcomes for these models are summarized in Table 1. We find that CSR consistently achieves the highest scores across all tasks, demonstrating its capability to promptly detect and adapt to environmental changes. In contrast, other baseline methods struggle to adjust to the introduction of the new friction variable.

Atari Experiments. We also conduct a series of interesting experiments on the Atari 100K games. Considering that we focus on games that have at least two distinct modes and two difficulty levels, we select five representative games for evaluation: Alien, Bank Heist, Carzy Climber, Gopher, and Pong. For each of these games, we perform experiments among a sequence of four tasks, where each task randomly assigns a (mode, difficulty) pair. For the source task \mathcal{M}_1 , we train these models for 400k steps. For tasks \mathcal{M}_2 to \mathcal{M}_4 , we limit the model adjustment to only 100k steps. We record the average final scores across these tasks and summarize them it Table 2. We see that CSR achieves the highest mean scores in all the five games. Moreover, Fig. A.7 illustrates the average generalization performance of various methods on downstream target tasks, while Fig. A.8 to Fig. A.12 present the training curves for each game, respectively. We observe that model-based methods tend to generalize more quickly than model-free ones. This finding suggests that the forward-planning capabilities of world models benefit in adapting to the dynamic changes in the Atari environment.

Ablation Study. To further explore the differences among various expansion strategies, we conduct experiments using the three methods described in Section 3.2 across simulation, CartPole, and Atari games, respectively. The results in Fig. 3(b) demonstrate that seeking for the optimal structure significantly improves expansion performance, leading us to apply the *Self-Adaptive* approach in

all our experiments. However, we also observe that each search step requires extensive training time for models with different expansion scales, making the search process highly time-consuming. For instance, it takes hours to perform searches in the Atari games (as a reference, training a world model from scratch takes about a day). Therefore, it is crucial to consider this trade-off in practical applications. Furthermore, we also investigate the impact of causal graph pruning on generalization ability. The two training curves depicted in Figure 3(c) illustrate the performance of CSR with and without causal structures on the Pong game. We observe a significantly faster and higher increase in the cumulative reward when taking structural relationships into consideration. This demonstrates the efficiency enhancement in policy learning through the removal of redundant causal variables, which accelerates the extraction and utilization of knowledge during the generalization process.

5 Related Work

In recent years, extensive research efforts have been invested in learning abstract representations in RL, employing diverse methodologies such as image reconstruction [41], contrastive learning [42, 43], and the development of world models [44]. A prominent research avenue within this domain is causal representation learning, which aims to identify high-level causal variables from low-level observations, thereby enhancing the accuracy of information available for decision-making processes [19]. Approaches such as ASRs [20] and IFactor [23] leverage causal factorization and structural constraints within causal variables to develop more accurate world models. Moreover, CDL [21] and GRADER [22] seek to boost exploration efficiency by learning causal models. Despite these advancements, many of these studies are tailored to specific tasks and struggle to achieve the level of generalization across tasks where human performance is notably superior [16].

To overcome these limitations, Harutyunyan et al. [9] develop a reward-shaping function that captures the target task’s information to guide policy learning. Taylor et al. [11] and Zhang et al. [12] aim to map tasks to invariant state variables, thereby learning policies robust to environmental changes. AdaRL [14] is dedicated to learning domain-shared and domain-specific representations to facilitate policy transfer. Distinct from these works, CSP [15] approaches from the perspective of policy learning directly, by incrementally constructing a subspace of policies to train agents. However, most of these works assume a constant state space, which is often not the case in practical applications. Therefore, in this paper, we investigate the feasibility of knowledge transfer when the state space can also change. Furthermore, the approach we propose is also related to the area of dynamic neural networks, where various methods have been developed to address sequences of tasks that require dynamical modifications to the network architecture, such as DEN [32], PackNet [45], APD [46], CPG [47], and Learn-to-Grow [33].

6 Conclusions and Future Work

In this paper, we explore a broader range of scenarios for generalizable reinforcement learning, where changes across domains arise not only from distribution shifts but also space expansions. We introduce a Causality-Guided Self-Adaptive Representation-based method (CSR) to investigate the adaptability of RL methods in these challenging scenarios. This approach uses a three-step strategy that enables agents to detect environmental changes and autonomously adjust as needed. Empirical results from various complex environments, such as CartPole and Atari games, demonstrate the effectiveness of our proposed method in generalizing across evolving tasks. The primary limitation of this work is that it only considers generalization across domains and does not account for nonstationary changes over time. Therefore, a future research direction is to develop methods to automatically detect and characterize nonstationary changes both over time and across tasks.

References

- [1] Kai Arulkumaran, Marc Peter Deisenroth, Miles Brundage, and Anil Anthony Bharath. Deep reinforcement learning: A brief survey. *IEEE Signal Processing Magazine*, 34(6):26–38, November 2017. ISSN 1053-5888.
- [2] David Silver, Aja Huang, Chris J Maddison, Arthur Guez, Laurent Sifre, George Van Den Driessche, Julian Schrittwieser, Ioannis Antonoglou, Veda Panneershelvam, Marc Lanctot, et al. Mas-

- tering the game of go with deep neural networks and tree search. *nature*, 529(7587):484–489, 2016.
- [3] Piotr Mirowski, Razvan Pascanu, Fabio Viola, Hubert Soyer, Andrew J Ballard, Andrea Banino, Misha Denil, Ross Goroshin, Laurent Sifre, Koray Kavukcuoglu, et al. Learning to navigate in complex environments. *arXiv preprint arXiv:1611.03673*, 2016.
- [4] J. Pearl and D. Mackenzie. *The Book of Why: The New Science of Cause and Effect*. Basic Books, 2018. ISBN 978-0-465-09761-6.
- [5] Shane Legg and Marcus Hutter. Universal intelligence: A definition of machine intelligence. *Minds and machines*, 17:391–444, 2007.
- [6] Robert Kirk, Amy Zhang, Edward Grefenstette, and Tim Rocktäschel. A survey of zero-shot generalisation in deep reinforcement learning. *Journal of Artificial Intelligence Research*, 76: 201–264, January 2023. ISSN 1076-9757.
- [7] Zhuangdi Zhu, Kaixiang Lin, Anil K Jain, and Jiayu Zhou. Transfer learning in deep reinforcement learning: A survey. *IEEE Transactions on Pattern Analysis and Machine Intelligence*, 2023.
- [8] Grégoire Mesnil, Yann Dauphin, Xavier Glorot, Salah Rifai, Yoshua Bengio, Ian Goodfellow, Erick Lavoie, Xavier Muller, Guillaume Desjardins, David Warde-Farley, et al. Unsupervised and transfer learning challenge: a deep learning approach. In *Proceedings of ICML Workshop on Unsupervised and Transfer Learning*, pages 97–110. JMLR Workshop and Conference Proceedings, 2012.
- [9] Anna Harutyunyan, Sam Devlin, Peter Vrancx, and Ann Nowé. Expressing arbitrary reward functions as potential-based advice. In *Proceedings of the AAAI conference on artificial intelligence*, volume 29, 2015.
- [10] Andrea Tirinzoni, Mattia Salvini, and Marcello Restelli. Transfer of samples in policy search via multiple importance sampling. In *International Conference on Machine Learning*, pages 6264–6274. PMLR, 2019.
- [11] Matthew E Taylor, Peter Stone, and Yaxin Liu. Transfer learning via inter-task mappings for temporal difference learning. *Journal of Machine Learning Research*, 8(9), 2007.
- [12] Amy Zhang, Rowan McAllister, Roberto Calandra, Yarin Gal, and Sergey Levine. Learning invariant representations for reinforcement learning without reconstruction. *arXiv preprint arXiv:2006.10742*, 2020.
- [13] Xue Bin Peng, Erwin Coumans, Tingnan Zhang, Tsang-Wei Lee, Jie Tan, and Sergey Levine. Learning agile robotic locomotion skills by imitating animals. *arXiv preprint arXiv:2004.00784*, 2020.
- [14] Biwei Huang, Fan Feng, Chaochao Lu, Sara Magliacane, and Kun Zhang. Adarl: What, where, and how to adapt in transfer reinforcement learning. *arXiv preprint arXiv:2107.02729*, 2021.
- [15] Jean-Baptiste Gaya, Thang Doan, Lucas Caccia, Laure Soulier, Ludovic Denoyer, and Roberta Raileanu. Building a subspace of policies for scalable continual learning. *arXiv preprint arXiv:2211.10445*, 2022.
- [16] Matthew E Taylor and Peter Stone. Transfer learning for reinforcement learning domains: A survey. *Journal of Machine Learning Research*, 10(7), 2009.
- [17] Kaiyang Zhou, Ziwei Liu, Yu Qiao, Tao Xiang, and Chen Change Loy. Domain generalization: A survey. *IEEE Transactions on Pattern Analysis and Machine Intelligence*, 45(4):4396–4415, 2023.
- [18] Yangyi Lu, Amirhossein Meisami, and Ambuj Tewari. Causal markov decision processes: Learning good interventions efficiently, 2021.

- [19] Bernhard Schölkopf, Francesco Locatello, Stefan Bauer, Nan Rosemary Ke, Nal Kalchbrenner, Anirudh Goyal, and Yoshua Bengio. Toward causal representation learning. *Proceedings of the IEEE*, 109(5):612–634, 2021.
- [20] Biwei Huang, Chaochao Lu, Liu Leqi, José Miguel Hernández-Lobato, Clark Glymour, Bernhard Schölkopf, and Kun Zhang. Action-sufficient state representation learning for control with structural constraints. In *International Conference on Machine Learning*, pages 9260–9279. PMLR, 2022.
- [21] Zizhao Wang, Xuesu Xiao, Zifan Xu, Yuke Zhu, and Peter Stone. Causal dynamics learning for task-independent state abstraction. *arXiv preprint arXiv:2206.13452*, 2022.
- [22] Wenhao Ding, Haohong Lin, Bo Li, and Ding Zhao. Generalizing goal-conditioned reinforcement learning with variational causal reasoning. *Advances in Neural Information Processing Systems*, 35:26532–26548, 2022.
- [23] Yu-Ren Liu, Biwei Huang, Zhengmao Zhu, Honglong Tian, Mingming Gong, Yang Yu, and Kun Zhang. Learning world models with identifiable factorization. *arXiv preprint arXiv:2306.06561*, 2023.
- [24] David Ha and Jürgen Schmidhuber. World models. *arXiv preprint arXiv:1803.10122*, 2018.
- [25] Danijar Hafner, Timothy Lillicrap, Mohammad Norouzi, and Jimmy Ba. Mastering atari with discrete world models. *arXiv preprint arXiv:2010.02193*, 2020.
- [26] AmirEmad Ghassami, Negar Kiyavash, Biwei Huang, and Kun Zhang. Multi-domain causal structure learning in linear systems. *Advances in neural information processing systems*, 31, 2018.
- [27] Weiran Yao, Guangyi Chen, and Kun Zhang. Temporally disentangled representation learning. *Advances in Neural Information Processing Systems*, 35:26492–26503, 2022.
- [28] Danijar Hafner, Jurgis Pasukonis, Jimmy Ba, and Timothy Lillicrap. Mastering diverse domains through world models. *arXiv preprint arXiv:2301.04104*, 2023.
- [29] Kun Zhang, Mingming Gong, Petar Stojanov, Biwei Huang, Qingsong Liu, and Clark Glymour. Domain adaptation as a problem of inference on graphical models. *Advances in neural information processing systems*, 33:4965–4976, 2020.
- [30] Khimya Khetarpal, Matthew Riemer, Irina Rish, and Doina Precup. Towards continual reinforcement learning: A review and perspectives. *Journal of Artificial Intelligence Research*, 75: 1401–1476, 2022.
- [31] Zhaohan Daniel Guo, Bernardo Avila Pires, Bilal Piot, Jean-Bastien Grill, Florent Altché, Rémi Munos, and Mohammad Gheshlaghi Azar. Bootstrap latent-predictive representations for multitask reinforcement learning. In *International Conference on Machine Learning*, pages 3875–3886. PMLR, 2020.
- [32] Jaehong Yoon, Eunho Yang, Jeongtae Lee, and Sung Ju Hwang. Lifelong learning with dynamically expandable networks. *arXiv preprint arXiv:1708.01547*, 2017.
- [33] Xilai Li, Yingbo Zhou, Tianfu Wu, Richard Socher, and Caiming Xiong. Learn to grow: A continual structure learning framework for overcoming catastrophic forgetting. In *International Conference on Machine Learning*, pages 3925–3934. PMLR, 2019.
- [34] Ju Xu and Zhanxing Zhu. Reinforced continual learning. *Advances in Neural Information Processing Systems*, 31, 2018.
- [35] Jiji Zhang and Peter Spirtes. Intervention, determinism, and the causal minimality condition. *Synthese*, 182:335–347, 2011.
- [36] Greg Brockman, Vicki Cheung, Ludwig Pettersson, Jonas Schneider, John Schulman, Jie Tang, and Wojciech Zaremba. Openai gym, 2016.

- [37] Marlos C Machado, Marc G Bellemare, Erik Talvitie, Joel Veness, Matthew Hausknecht, and Michael Bowling. Revisiting the arcade learning environment: Evaluation protocols and open problems for general agents. *Journal of Artificial Intelligence Research*, 61:523–562, 2018.
- [38] Volodymyr Mnih, Koray Kavukcuoglu, David Silver, Andrei A Rusu, Joel Veness, Marc G Bellemare, Alex Graves, Martin Riedmiller, Andreas K Fidjeland, Georg Ostrovski, et al. Human-level control through deep reinforcement learning. *nature*, 518(7540):529–533, 2015.
- [39] Max Schwarzer, Ankesh Anand, Rishab Goel, R Devon Hjelm, Aaron Courville, and Philip Bachman. Data-efficient reinforcement learning with self-predictive representations. *arXiv preprint arXiv:2007.05929*, 2020.
- [40] Weirui Ye, Shaohuai Liu, Thanard Kurutach, Pieter Abbeel, and Yang Gao. Mastering atari games with limited data. *Advances in neural information processing systems*, 34:25476–25488, 2021.
- [41] Manuel Watter, Jost Springenberg, Joschka Boedecker, and Martin Riedmiller. Embed to control: A locally linear latent dynamics model for control from raw images. *Advances in neural information processing systems*, 28, 2015.
- [42] Pierre Sermanet, Corey Lynch, Yevgen Chebotar, Jasmine Hsu, Eric Jang, Stefan Schaal, Sergey Levine, and Google Brain. Time-contrastive networks: Self-supervised learning from video. In *2018 IEEE international conference on robotics and automation (ICRA)*, pages 1134–1141. IEEE, 2018.
- [43] Bogdan Mazouze, Remi Tachet des Combes, Thang Long Doan, Philip Bachman, and R Devon Hjelm. Deep reinforcement and infomax learning. *Advances in Neural Information Processing Systems*, 33:3686–3698, 2020.
- [44] Ramanan Sekar, Oleh Rybkin, Kostas Daniilidis, Pieter Abbeel, Danijar Hafner, and Deepak Pathak. Planning to explore via self-supervised world models. In *International Conference on Machine Learning*, pages 8583–8592. PMLR, 2020.
- [45] Arun Mallya and Svetlana Lazebnik. Packnet: Adding multiple tasks to a single network by iterative pruning. In *Proceedings of the IEEE conference on Computer Vision and Pattern Recognition*, pages 7765–7773, 2018.
- [46] Jaehong Yoon, Saehoon Kim, Eunho Yang, and Sung Ju Hwang. Scalable and order-robust continual learning with additive parameter decomposition. *arXiv preprint arXiv:1902.09432*, 2019.
- [47] Ching-Yi Hung, Cheng-Hao Tu, Cheng-En Wu, Chien-Hung Chen, Yi-Ming Chan, and Chu-Song Chen. Compacting, picking and growing for unforgetting continual learning. *Advances in Neural Information Processing Systems*, 32, 2019.
- [48] Razvan V Florian. Correct equations for the dynamics of the cart-pole system. *Center for Cognitive and Neural Studies (Coneural), Romania*, page 63, 2007.
- [49] Danijar Hafner, Timothy Lillicrap, Ian Fischer, Ruben Villegas, David Ha, Honglak Lee, and James Davidson. Learning latent dynamics for planning from pixels. In *International conference on machine learning*, pages 2555–2565. PMLR, 2019.

A Proofs of Identifiability Theory

Before presenting the proofs of identifiability theory, we first introduce the relevant notations and assumptions, related to Huang et al. [14], Yao et al. [27], Liu et al. [23].

Notations. We denote the underlying state variable by $\mathbf{s}_t = \{s_{1,t}, \dots, s_{d,t}\}$ and denote o_t as the observation. Also, we denote the mapping from state estimator $\hat{\mathbf{s}}_t$ to state \mathbf{s}_t by $\mathbf{s}_t = h(\hat{\mathbf{s}}_t)$, and denote the Jacobian matrix of h as \mathbf{H}_t . Let $\zeta \triangleq \log p(s_{k,t} | \mathbf{s}_{t-1})$, we further denote

$$\boldsymbol{\omega}_{k,t} \triangleq \left(\frac{\partial^2 \zeta_{k,t}}{\partial s_{k,t} \partial s_{1,t-1}}, \frac{\partial^2 \zeta_{k,t}}{\partial s_{k,t} \partial s_{2,t-1}}, \dots, \frac{\partial^2 \zeta_{k,t}}{\partial s_{k,t} \partial s_{d,t-1}} \right)^\top, \hat{\boldsymbol{\omega}}_{k,t} \triangleq \left(\frac{\partial^3 \zeta_{k,t}}{\partial s_{k,t}^2 \partial s_{1,t-1}}, \frac{\partial^3 \zeta_{k,t}}{\partial s_{k,t}^2 \partial s_{2,t-1}}, \dots, \frac{\partial^3 \zeta_{k,t}}{\partial s_{k,t}^2 \partial s_{d,t-1}} \right)^\top. \quad (\text{A.1})$$

Assumption 1. The data generation process at each time t can be described by:

$$\begin{cases} o_t &= g^o(\mathbf{s}_t) \\ r_t &= g^r(\mathbf{s}_{t-1}, \epsilon_t^r) \\ \mathbf{s}_t &= g^s(\mathbf{s}_{t-1}, a_{t-1}, \epsilon_t^s), \end{cases} \quad (\text{A.2})$$

where g^o is the observation function, g^r represents the reward function, g^s is the transition function, and the $\epsilon_t^s, \epsilon_t^r$ terms are corresponding independent and identically distributed (i.i.d.) random noises. We assume that g^o, g^r, g^s are invertible.

Assumption 2. ζ is twice differentiable with respect to $s_{k,t}$ and differentiable with respect to $s_{l,t-1}$, for all $l \in \{1, \dots, d\}$.

A.1 Proof of Theorem 1

Based on aforementioned assumptions and definitions, Theorem 1 establishes the conditions for the identifiability of the state variable \mathbf{s}_t and the structural matrices D in Eq. (1).

Theorem 1. (Identifiability of world model in Eq. (1)). Suppose there exist mappings g^o and h such that $o_t = g^o(\mathbf{s}_t)$ and $\mathbf{s}_t = h(\hat{\mathbf{s}}_t)$. If the following conditions are satisfied, then \mathbf{s}_t is identifiable up to nonlinear invertible component-wise transformations: (1) g^o is invertible; (2) for any $k_1, k_2 \in \{1, \dots, d\}$ and $k_1 \neq k_2$, $\hat{\mathbf{s}}_{k_1,t}$ and $\hat{\mathbf{s}}_{k_2,t}$ are conditionally independent given $\hat{\mathbf{s}}_{t-1}$; (3) for every possible value of \mathbf{s}_t , the vector functions defined in Eq. (A.1) are linearly independent (see Yao et al. [27], Liu et al. [23]). Furthermore, if the Markov condition and faithfulness assumption hold, then the structural matrices D are also identifiable (see Huang et al. [14]).

The proofs for it have already been provided in existing work. In order to better support the proofs of Theorem 2, Theorem 3, and Corollary 1, we first summarize the proof steps of the identifiability of the state variables \mathbf{s}_t for Theorem 1, following Yao et al. [27] and Liu et al. [23], which are:

- In step 1, by making use of the conditional independence of the components of $\hat{\mathbf{s}}_t$ given $\hat{\mathbf{s}}_{t-1}$, it is shown that:

$$\frac{\partial^2 \log p(\hat{\mathbf{s}}_t | \hat{\mathbf{s}}_{t-1})}{\partial \hat{s}_{i,t} \partial \hat{s}_{j,t}} = 0. \quad (\text{A.3})$$

- In step 2, by utilizing the Jacobian matrix \mathbf{H}_t to calculate Eq. (A.3), it is derived that

$$\frac{\partial^3 \log p(\hat{\mathbf{s}}_t | \hat{\mathbf{s}}_{t-1})}{\partial \hat{s}_{i,t} \partial \hat{s}_{j,t} \partial s_{l,t-1}} = \sum_{k=1}^d \left(\frac{\partial^3 \zeta_{k,t}}{\partial s_{k,t}^2 \partial s_{l,t-1}} \cdot \mathbf{H}_{k,i,t} \mathbf{H}_{k,j,t} + \frac{\partial^2 \zeta_{k,t}}{\partial s_{k,t} \partial s_{l,t-1}} \cdot \frac{\partial \mathbf{H}_{k,i,t}}{\partial \hat{s}_{j,t}} \right) \equiv 0. \quad (\text{A.4})$$

- In step 3, it is established that \mathbf{s}_t is identifiable, up to an invertible, component-wise nonlinear transformation of a permuted version of $\hat{\mathbf{s}}_t$, if the linear independence of vector functions defined in A.1 holds and the the Jacobian matrix \mathbf{H}_t satisfies Eq. (A.4).

Following these steps, below we provide the proofs of Theorem 2, Theorem 3, and Corollary 1.

A.2 Proof of Theorem 2

Different from existing methods, to capture the changing dynamics in the environment, we have introduced a task-specific change factor, θ_i , into the world model as defined in Eq. (2). Accordingly, Theorem 2 presents the identifiability of θ_i and the corresponding structural matrices $D^{\theta_i \rightarrow \cdot}$ for scenarios involving only distribution shifts.

Theorem 2. (Identifiability of θ_i in Eq. (2)). Suppose the data generation process encounters distribution shifts as described in Eq. (2). If \mathbf{s}_t and the generative functions g^o , g^r , g^s , defined in Eq. (A.2), are identified, then θ_i and the corresponding structural matrices $D^{\theta_i \rightarrow \cdot}$ are identifiable.

Proof. The proof of identifiability for the structural matrix $D^{\theta_i \rightarrow \cdot}$ has already been provided in Huang et al. [14]. Next, we prove that θ_i can also be identified in the following four steps:

- In step 1, we show that θ_i^s can be identified when only the transition function undergoes distribution shifts.
- In step 2, we demonstrate that θ_i^r is identifiable when only the reward function experiences distribution shifts.
- In step 3, we prove that θ_i^o can be identified when only the observation function exhibits distribution shifts.
- In step 4, we establish that in the general case, where the observation, reward, and transition functions may undergo distribution shifts simultaneously, $\theta_i = \{\theta_i^o, \theta_i^r, \theta_i^s\}$ is identifiable.

Step 1: prove the identifiability of θ_i^s .

When only the transition function undergoes distribution shifts, it can be reformulated from Eq. (A.2) as follows:

$$\mathbf{s}_t = g^s(\mathbf{s}_{t-1}, a_{t-1}, \theta_i^s, \epsilon_t^s) \quad (\text{A.5})$$

Note that the state \mathbf{s}_t is directly determined by the previous state \mathbf{s}_{t-1} , the action a_{t-1} , and the change factor θ_i^s via the transition function g^s . This direct dependence implies that the identifiability of θ_i^s relies on both the state variable \mathbf{s}_t and the action a_{t-1} . Since \mathbf{s}_t has already been identified, action a_{t-1} is observable, and g^s is invertible, we can conclude that θ_i^s is identifiable.

Step 2: prove the identifiability of θ_i^r .

If the environment only experiences distribution shifts on the reward function, we can reformulate it as:

$$r_t = g^r(\mathbf{s}_{t-1}, \theta_i^r, \epsilon_t^r). \quad (\text{A.6})$$

Similarly, in this function, we have identified \mathbf{s}_{t-1} , and observed reward r_t . Since g^r is assumed to be invertible, we can identify θ_i^r .

Step 3: prove the identifiability of θ_i^o .

Let $\hat{\theta}_i^o$ denotes the estimation for θ_i^o . If only the observation function exhibits distribution shifts, we can rewrite it as:

$$o_t = g^o(\mathbf{s}_t, \theta_i^o). \quad (\text{A.7})$$

Likewise, we can derive the following equation for the estimator $\hat{\theta}_i^o$:

$$o_t = g^o(\mathbf{s}_t, \hat{\theta}_i^o). \quad (\text{A.8})$$

Therefore, consider o_t is observed, \mathbf{s}_t and g^o have been identified, we have

$$\hat{\theta}_i^o \equiv \theta_i^o \quad (\text{A.9})$$

That is, θ_i^o is identifiable.

Step 4: prove the identifiability of θ_i in the general case.

This step can be easily demonstrated by combining the proofs above. □

A.3 Proof of Theorem 3

In Theorem 3, we focus on the identifiability of the newly added variables $\mathbf{s}_t^{\text{add}}$ and their corresponding structural matrices, when the state space is expanded by incorporating additional dimensions.

Theorem 3. (Identifiability of Expanded State Space). Consider the expansion of the state space \mathcal{S} by incorporating additional dimensions. Suppose \mathbf{s}_t has already been identified according to Theorem 1, the identifiability of the newly added variables $\mathbf{s}_t^{\text{add}}$ and the additional structural matrices, i.e., $D^{\mathbf{s}^{\text{add}} \rightarrow \cdot}$ and $D^{\cdot \rightarrow \mathbf{s}^{\text{add}}}$, can be established if $\mathbf{s}_t^{\text{add}}$ (1) represents a differentiable function of the observations o_t , i.e., $\mathbf{s}_t^{\text{add}} = f(o_t)$, and (2) fulfills conditions (2) and (3) specified in Theorem 1.

Experiments	<i>Random</i>	<i>Deterministic</i>	<i>Self-Adaptive</i>
Simulated	4.0	5.0	4.2
Cartpole	6.2	6.0	4.0
Atari	7.8	8.0	6.4

Table A.1: The expansion results of different methods in our experiments.

Proof. For the newly added variables, since they also satisfy condition (2) of Theorem 1, we can derive the same properties as described in Eq. (A.3) and Eq. (A.4) by following steps 1 and 2 in the proof of Theorem 1. Additionally, since the vector equation corresponding to s_t^{add} also satisfies linear independence condition, it is straightforward that s_t^{add} can also be identified. As for the additional structural matrices introduced, the Markov condition and faithfulness assumptions required for their identifiability have already been demanded in the identifiability properties of the existing structural matrices, thus no additional proof is needed. \square

Corollary 1. (*Identifiability under Multiple Shifts*). *Assume the data generation process involves both distribution shifts and state space shifts that comply with Theorem 2 and Theorem 3, respectively. In this case, both the domain-specific factor θ and the newly added state variable s_t^{add} are identifiable, up to permutation and nonlinear invertible, component-wise transformations.*

Proof. Since the conditions for the identifiability of the newly added variables s_t^{add} and the change factor θ_i do not affect each other, Corollary 1 can be directly derived from the conclusions of Theorems 1, 2 and 3. \square

B Self-Adaptive Expansion Strategy

We design three different approaches for the State Space Expansion step: *Random*, *Deterministic*, and *Self-Adaptive*. In *Random*, the number of causal variables expanded is randomly chosen. Table A.1 shows the selection range varying across different tasks. For *Deterministic*, we follow the approach used in DEN [32], first adding a predefined number of variables to the causal graph and then applying group sparsity regularization to the network parameters corresponding to the newly added variables. Table A.1 provides the final expansion results of *Deterministic* across these three tasks. Next, we introduce the *Self-Adaptive* method.

Different from prior methods, *Self-Adaptive* integrates state space expansion into the reinforcement learning framework. To achieve this, the first thing that needs to be done is to transform the expansion concept into a decision-making process. Since our goal is to determine how many causal variables should be incorporated into the causal graph, the action u_t can be intuitively represented as the number of variables to add. Regarding the state variable v_t , it is designed to reflect the current state of the system. Given that the model’s expansion is inseparable from its original structure and adaptability to the target task \mathcal{M}_i , we formulate the state variable as a reflection of both the original network size and its predictive capability on \mathcal{M}_i , denoted as $v_t = (x_t, \Delta_\tau)$. To be specific, $x_t = (x_t^o, x_t^r, x_t^s)$, where x_t^o , x_t^r , and x_t^s represent the combination of the number of nodes for each layer in the models defined in Eq. (2), respectively. If the transition model is an m -layer network, then x_t^s is an m -dimensional vector, with the l -th element representing the number of nodes in the l -th layer. Moreover, $\Delta_\tau = \tau - \tau^*$ represents the difference between the model’s predictive performance τ and the threshold τ^* .

Whenever the controller takes an action u_t , we correspondingly extend the model by augmenting it with additional components, and train the newly added parts from scratch with a few amount of data. For instance, if $u_t = d'$, it implies that d' causal state variables will be incorporated. Then for the observation model, we only need to focus on learning the mapping from s_t^{add} to o_t , together with the structural constraints $D^{s_t^{\text{add}} \rightarrow o}$. A similar principle applies to the reward and transition model. Finally, we re-estimate the performance of the expanded model, denoted as τ'_t , and derive the reward as:

$$r_t = (\tau - \tau'_t) - \lambda_r u_t, \quad (\text{A.10})$$

where $\tau - \tau'_t$ reflects the change in the model’s representational capacity before and after expansion, the term $-\lambda_r u_t$ acts as a regularization penalty that imposes a cost on model expansion, and λ_r is the corresponding scaling factor.

Simulated Environment	Architecture	Hyper Parameters
Change factor θ^s	-	Uniform, [-1, 1]
Random noise ϵ_t^s	-	Gaussian, $\mathcal{N}(0, 0.2I)$
Reward function g^r	Dense	128, he uniform, relu
	Dense	64, he uniform, relu
	Dense	1, glorot uniform
Transition function g^s	Dense	4, glorot uniform, tanh
Observation function g^o	Dense	128, glorot uniform

Table A.2: Architecture and hyperparameters for the simulated environment.

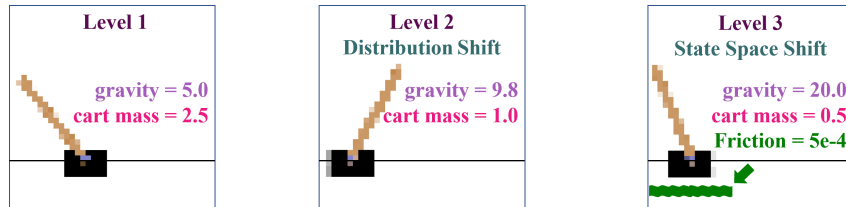


Figure A.1: An illustration of Cartpole environment.

Building upon the above foundation, it becomes feasible to develop and train a policy aimed at dynamically enhancing the causal model in adaptation to current task \mathcal{M}_i through strategic expansion. Table A.1 presents the optimal actions identified by *Self-Adaptive* during the experiments, where the action range is identical to that of *Random*. The integration of the Distribution Shifts Detection step and the State Space Expansion step allows the model to autonomously decide whether it is necessary to expand the state space, and to self-adaptively choose the appropriate scale for expansion.

C Complete Experimental Details

C.1 Simulated Environment

We construct the simulated environment based on the following POMDP framework:

$$\begin{aligned}
 s_1 &\sim \mathcal{N}(0, I_0), \\
 o_t &= g^o(s_{t-1}), \\
 s_t &= g^s(\theta^s, s_{t-1}, a_{t-1}) + \epsilon_t^s, \quad \epsilon_t^s \sim \mathcal{N}(0, I_\epsilon) \\
 r_t &= g^r(s_{t-1}),
 \end{aligned} \tag{A.11}$$

where s_1 and ϵ_t^s are sampled from Gaussian distributions, and functions g^o , g^s , and g^r are implemented using MLPs. To simulate scenarios of distribution shifts, we generate random values for θ^s in different tasks. To model changes in the state space \mathcal{S} , we randomly augment it with n dimensions, where n is uniformly sampled from the range [3,7]. Moreover, to introduce structural constraints into the data generation process, we initialize the network parameters for g^o , g^s , and g^r , by randomly dropping them out with a probability of 0.5. The network weights then remain constant throughout the learning process. For each task, agents are allowed to collect data over 100 episodes, each consisting of 256 time steps. Table A.2 provides the corresponding network architecture and hyperparameters.

C.2 CartPole Environment

Based on the conclusions in Florian [48], we modify the CartPole game to introduce changes in the distribution and state space. Specifically, for Task 1 and Task 2, the transition processes adhere to the

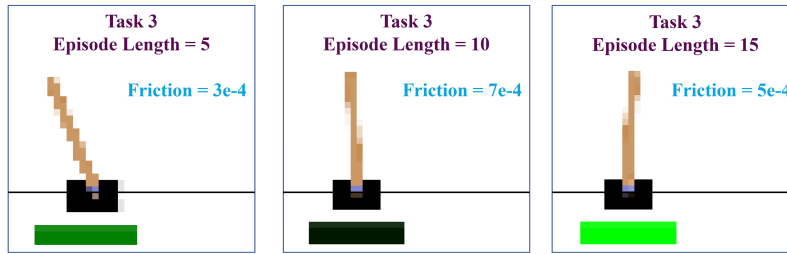


Figure A.2: An illustration of the CartPole game under different friction coefficients.

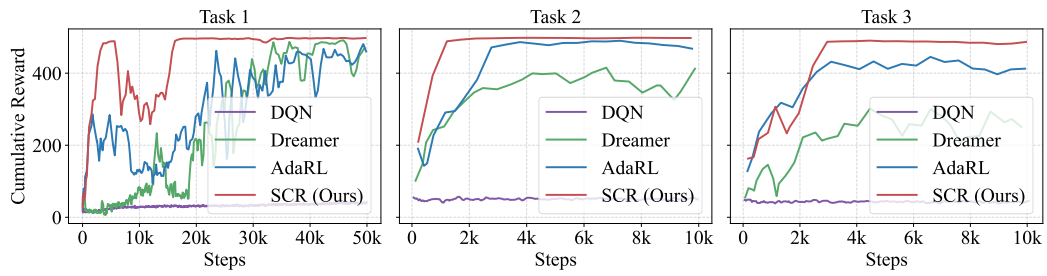


Figure A.3: Training results of CartPole experiments

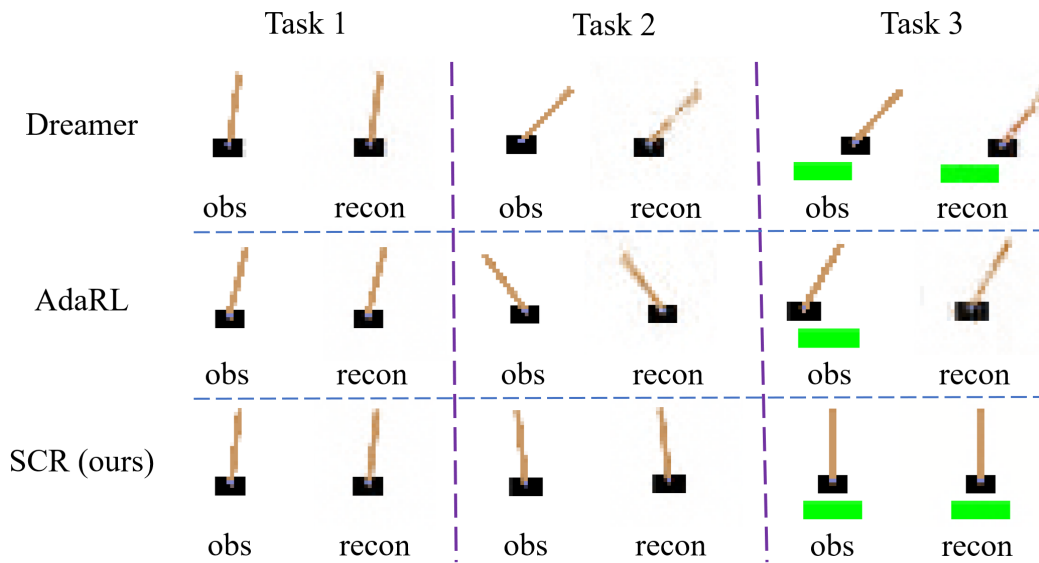


Figure A.4: The reconstructed observations of different world models in CartPole.

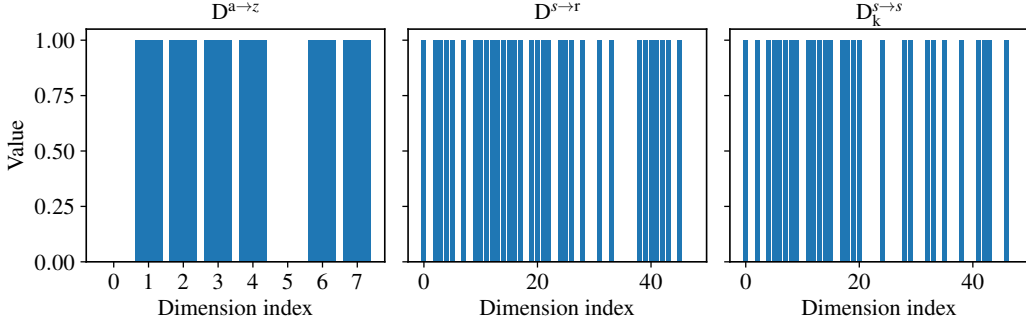


Figure A.5: Estimated causal structural matrices in CartPole.

following formulas:

$$\ddot{\psi} = \frac{g \sin \psi + \cos \psi \left(\frac{-F - m_p l \dot{\psi}^2 \sin \psi}{m_c + m_p} \right) - \frac{\mu_c \dot{\psi}}{m_p l}}{l \left(\frac{4}{3} - \frac{m_p \cos^2 \psi}{m_c + m_p} \right)} \quad (\text{A.12})$$

$$\ddot{x} = \frac{F + m_p l \left(\dot{\psi}^2 \sin \psi - \ddot{\psi} \cos \psi \right)}{m_c + m_p},$$

where the parameters used are the same as those defined in Section 2 of Florian [48], except that ψ is used in place of θ . By altering the values of m_c and g , we can simulate distribution shifts. For Task 3, we introduce the friction between the cart and the track into the game, denoted as μ_c , thus altering Eq. (A.12) to Eq. (21) and Eq. (22) in Florian [48], which is:

$$\ddot{\psi} = \frac{g \sin \psi + \cos \psi \left\{ \frac{-F - m_p l \dot{\psi}^2 [\sin \psi + \mu_c \operatorname{sgn}(N_c \dot{x}) \cos \psi]}{m_c + m_p} + \mu_c g \operatorname{sgn}(N_c \dot{x}) \right\} - \frac{\mu_c \dot{\psi}}{m_p l}}{l \left\{ \frac{4}{3} - \frac{m_p \cos \psi}{m_c + m_p} [\cos \psi - \mu_c \operatorname{sgn}(N_c \dot{x})] \right\}} \quad (\text{A.13})$$

$$\ddot{x} = \frac{F + m_p l \left(\dot{\psi}^2 \sin \psi - \ddot{\psi} \cos \psi \right) - \mu_c N_c \operatorname{sgn}(N_c \dot{x})}{m_c + m_p}.$$

Note that μ_c varies cyclically every 5 steps among $\{3e-4, 5e-4, 7e-4\}$, so that the agent must continually monitor it throughout the process to achieve higher and stable rewards. This helps us assess whether the agent has detected the newly introduced variable. Additionally, we also visualize these changes in the image inputs; Fig. A.2 presents examples under different friction coefficients. Our implementation is built upon Dreamer [25], Table A.3 lists the hyperparameters that are specifically set in our experiments. Fig. A.3 illustrates the corresponding training results. Moreover, Fig. A.4 shows a comparison of the reconstruction effects of different world models across the three tasks. Note that our implementation is based on Dreamer, where the transition model is an RSSM [49]. Consequently, we divide the state s_t into a deterministic state h_t and a stochastic state z_t . With this setup, the identified structural matrices in our experiment is shown in Fig. A.5.

C.3 Atari Environment

Atari serves as a classic benchmark in reinforcement learning, with most studies using it to evaluate the performance of proposed methods on fixed tasks. However, as mentioned in Machado et al. [37], many Atari tasks are quite similar, also allowing for the assessment of a reinforcement learning method’s generalization capabilities. Specifically, within the same game, we can adjust its modes and difficulty levels to alter the game dynamics. Although the goals of the game remain unchanged, increasing the complexity of modes and difficulty necessitates consideration of more variables, thus posing challenges for knowledge generalization. Fig. A.6 gives an example in Crazy Climber.

Therefore, according to Table 10 in Machado et al. [37], we select five games that feature different modes and levels of difficulty, and set the task sequence as four in our experiments. For Task 1, the

Hyper Parameters	Values in CartPole	Values in Atari
Action repeat	1	4
Batch size	20	16
Imagination horizon	8	15
Sequence length	30	64
Size of θ	2	20
Size of h_t	30	512
Size of z_t	4	32
Size of hidden nodes	100	512
Size of hidden layers	2	2

Table A.3: Hyperparameters of CSR for CartPole and Atari 100K games.

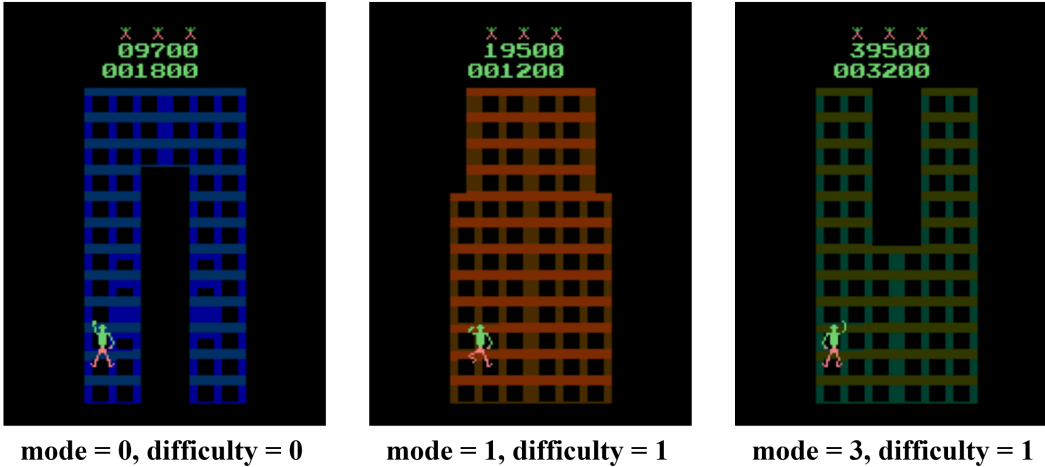


Figure A.6: Different modes of the game Crazy Climber.

agent is trained from scratch with 400k steps. For Tasks 2 to 4, different methods are employed to maximize the generalization of acquired knowledge to new tasks with 100k steps. Fig. A.8 to Fig. A.12 illustrates the training returns in these five games with different methods, Fig. A.7 are the average generalization performances, and Table A.3 lists the network parameters of CSR.

Furthermore, an interesting direction for future research is the exploration of the ability of RL methods to generalize across different games, such as Space Invaders and Demon Attack. These games feature distinct visuals but share similar gameplay and rules. While humans can easily transfer knowledge between these tasks, this remains a challenging feat for artificial intelligence. Additionally, investigating the relationship between generalization performance and task similarity presents a valuable research topic.

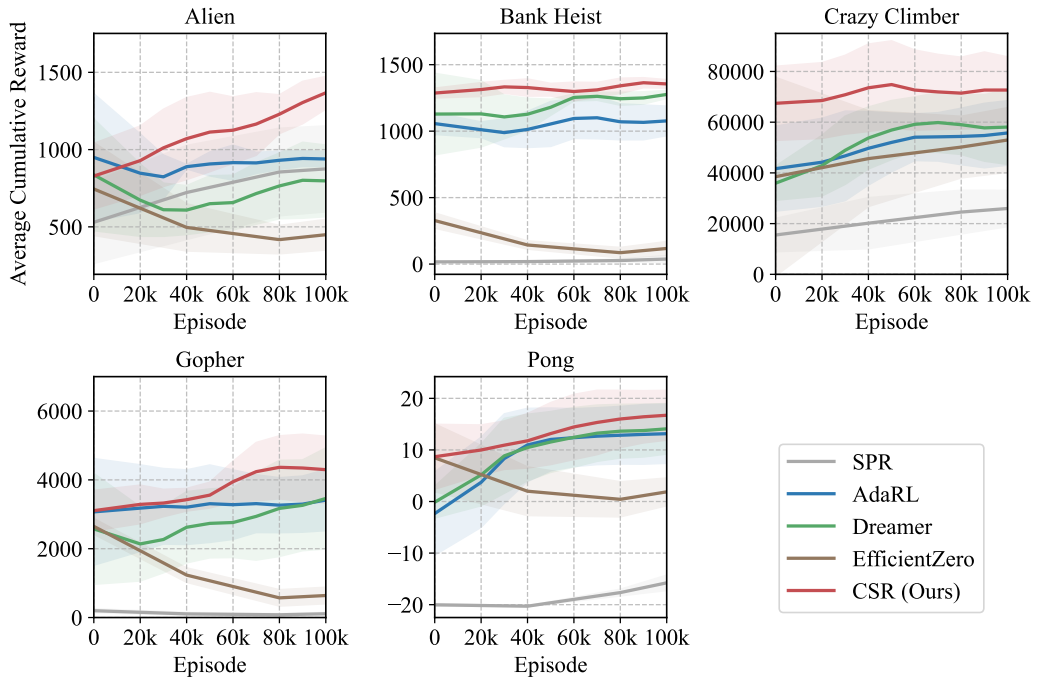


Figure A.7: Average generalization performance of different methods in Atari 100K games.

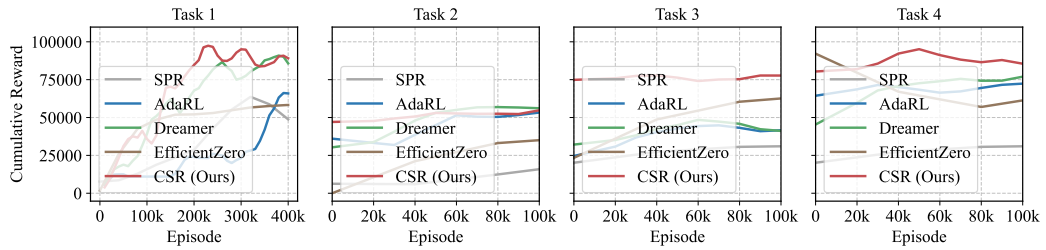


Figure A.8: Training results of different world models in game Crazy Climber.

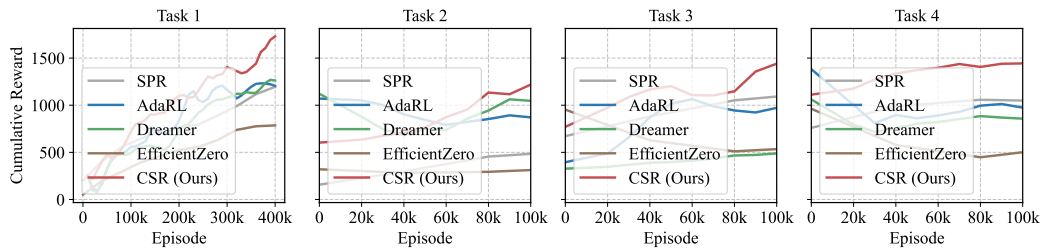


Figure A.9: Training results of different world models in game Alien.

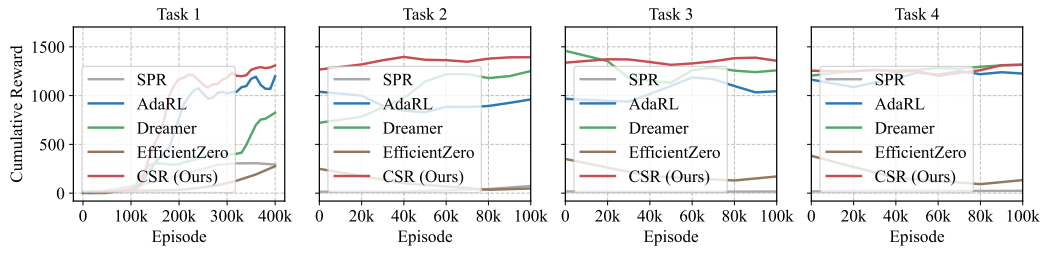


Figure A.10: Training results of different world models in game Bank Heist.

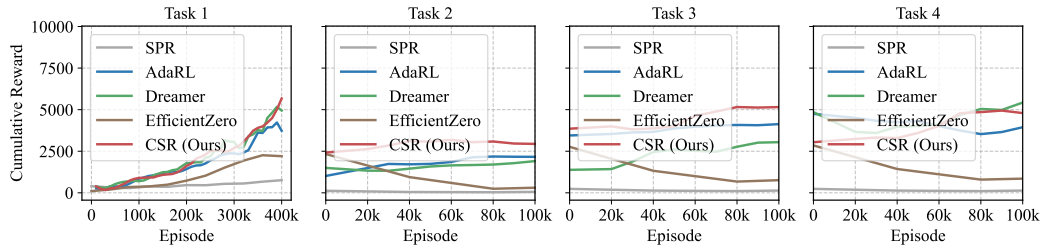


Figure A.11: Training results of different world models in game Gopher.

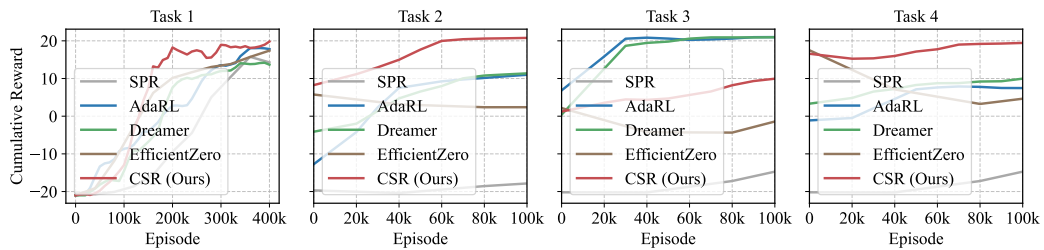


Figure A.12: Training results of different world models in game Pong.